

Pinpoint the jet apex in 3C 84

**G. F. Paraschos,^{a,*} J.-Y. Kim,^{b,a} T. P. Krichbaum,^a J. Oh,^c J. A. Hodgson,^{c,b}
M. A. Gurwell^d and J. A. Zensus^a**

^aMax-Planck-Institut für Radioastronomie, Auf dem Hügel 69, 53121, Bonn, Germany;

^bKorea Astronomy and Space Science Institute, 776 Daedeokdae-ro, Yuseong-gu, Daejeon 30455, Korea

^cDepartment of Physics and Astronomy, Sejong University, 209 Neungdong-ro, Gwangjin-gu, Seoul 05006, Korea

^dCenter for Astrophysics | Harvard & Smithsonian, 60 Garden Street, Cambridge, MA 02138, USA

E-mail: gfparaschos@mpi-fr-bonn.mpg.de

Jets which are powered by an AGN are a crucial element in the study of their central black holes (BH) and their immediate surroundings. The formation of such jets is the subject of intense research, mainly based on the dichotomy presented by the two main jet launching scenarios – the one from Blandford & Payne (1982), and the one from Blandford & Znajek (1977). In this work we study the prominent and nearby radio galaxy 3C 84 (NGC 1275) with 15, 43, and 86 GHz quasi-simultaneous VLBI observations. From these we determine the jet apex to be located $83 \pm 7 \mu\text{as}$ ($0.028 - 0.11 \text{ pc}$) upstream of the 86 GHz VLBI core, applying a two dimensional cross-correlation analysis. A byproduct of this analysis are spectral index maps, in which we identify a robust spectral index gradient in the north-south direction, for the first time at such high resolution, for the 43-86 GHz pair. The magnetic field strength at distances from the VLBI core comparable to measurements from the literature (~ 10 Schwarzschild radii) for other prominent AGN, like NGC 1052 and M 87, is computed to be 70 – 600 G. Implications for the magnetic field topology are also discussed.

*** European VLBI Network Mini-Symposium and Users' Meeting (EVN2021) ***

*** 12-14 July, 2021 ***

*** Online ***

*Speaker

1. Introduction – 3C 84 over the years

NGC 1275 is the central radio galaxy of the Perseus cluster. It harbours 3C 84, which is one of the brightest radio galaxies in the northern sky, making it a suitable target for high spatial resolution imaging with centimetre- and millimetre-VLBI. From radio to γ -rays, the source shows prominent flux variability (see Fig. 1). Its relation to the structural variability detected in the VLBI images is a topic of intense study. The first VLBI images of 3C 84 were published in the early 1950s [1]. Early cm- [2] and mm-VLBI maps [3, 4] already showcased the complexity of the jet both near the nucleus, as well as further downstream, in the $\sim 10 - 20$ mas region, where a complex and lobe-like structure is formed by the more extended emission. At 43 GHz and on the 3 mas scale three dominant emission regions, denoted with C1, C2, and C3 exist [5]. C1 is the nuclear region, C2 is the diffuse emission in the southwest of the nucleus and C3, which is a recently ejected component (~ 2005 [6]), travelling in a southern direction. Two major flux brightening events are known for 3C 84; one in the 1990's, which might be connected to the appearance of C2 and one in the 1960's [7] from which the $10 - 20$ mas diffuse emission in the south may originate.

The pronounced source activity likely has resulted in the two sided jets we are observing nowadays, with the southern jets being more prominent. The counter-jet is fainter and has been observed at 8, 22, 43 [8–10], and recently also at 86 GHz [11]. An optical thick free-free absorber (perhaps a torus) around the central engine has been proposed as a possible explanation for the lack of observable counter-jet emission on sub-mas scales [8, 9, 12].

Regarding the jet kinematics, components seem to advance in a dense medium at sub-luminal velocities ($\sim 0.1c$) and then accelerate further downstream to $0.3 - 0.5c$, with reported apparent velocities of up to $0.9c$ [4, 6, 8]. The components seem to follow curved trajectories [4, 13].

Flux peaks can usually be associated with component ejections and intense activity in the jet region. Figure 1 displays the radio and sub-mm flux density, together with γ -ray emission, of 3C 84 since 2011. The tight correspondence between the radio and sub-mm flux density is noticeable, with the intensity peaks in 2015 and 2017 apparently correlated with component ejections in the 0.5 mas region south of the VLBI core, seen both at 43, and 86 GHz observations (see Paraschos et al. in prep.).

3C 84 is also one of the very few TEV γ -ray emitting sources [6, 14, 15]. However, possible correlations between the γ -ray and radio flaring lack high significance (see Fig. 1).

2. Jet apex position

Quasi-simultaneous observations of 3C 84 were carried out at 15, 43, and 86 GHz in May 2015, with the Very Long Baseline Array (VLBA) and the Global Millimeter VLBI Array (GMVA). The simultaneity of the observations resulted in an unique opportunity to study the core shift of 3C 84 [18], and by extrapolation pinpoint the jet apex. For this study we used the already published images in [12]. In order to determine the core shift, we calculated the the distance of the intensity peaks of the core region, at 15 and 43 GHz, relative to the 86 GHz intensity peak (which we placed at the origin). This calculation was done by employing the standard two dimensional cross-correlation and determining where the cross-correlation coefficient peaked, for the 15-43 and 43-86 GHz pairs. For the alignment of the images, we chose optically thin, clearly defined regions, to perform the

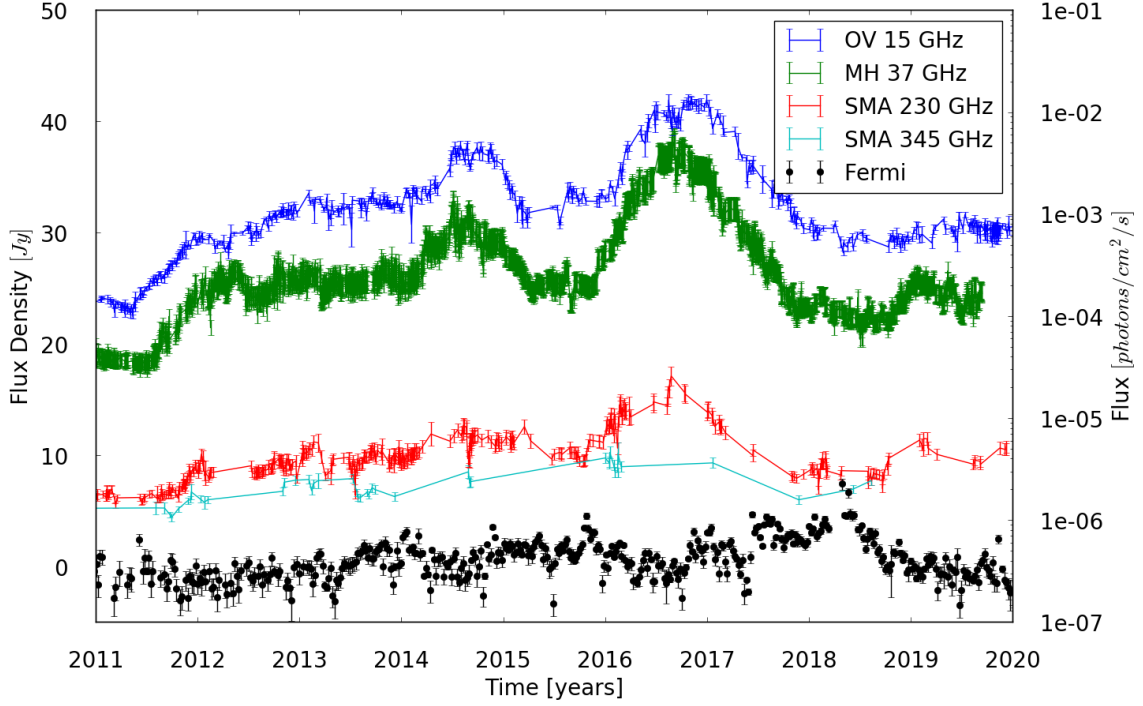


Figure 1: Radio flux of 3C 84 at 15 GHz (Owen’s Valley Radio Observatory, blue; see [16]), 37 GHz (Met-sähovi Radio Observatory, green), 230 GHz, and 345 GHz (Submillimeter Array, red and teal respectively), as well as the γ -ray flux (Fermi-LAT, black; see [17]) since the year 2011.

cross-correlation. Specifically, for the 15-43 GHz pair we used the C3 region, and for the 43-86 GHz pair the region ~ 1 mas south of the 86 GHz VLBI core. The distances as a function of the frequency are plotted in Fig. 2.

Following [19], we fitted a power law of the form:

$$\Delta r_{\text{core}} = r_0 \left(\left(\frac{\nu}{86\text{GHz}} \right)^{-1/k_r} - 1 \right) [\mu\text{as}], \quad (1)$$

where $k_r = [2n + b(3 - 2\alpha_{\text{thin}}) - 2]/(5 - 2\alpha_{\text{thin}})$, n and b are the particle number density and magnetic field strength power-law indices, respectively, and α_{thin} is the optically thin spectral index. With the physically motivated equipartition assumption that $k_r = 1$ [19–22], we find that the jet apex, and by extension the black hole of 3C 84 is at a distance of $83 \pm 7 \mu\text{as}$ upstream of the 86 GHz VLBI core (see Fig. 2), in good agreement with [23]. Our result, which is further supported by the position angle of the counter-jet reported at larger distances (see [8]), points to a different scenario than the one presented in [24]. In that work, the authors estimate a core shift of 0.03 mas from the 22 GHz VLBI core, under the assumption that the emission upstream of the core is the sub-mas counter-jet.

In Fig. 3 we plot the position of the intensity peaks of the core region at the three observed frequencies over image contours of the 86 GHz observations. The jet apex appears upstream, north-west of the 86 GHz intensity peak, at a position angle (P. A.) of $-20^\circ \pm 14^\circ$. Assuming a viewing angle in the $20^\circ - 65^\circ$ range [10, 25], the de-projected distance of the jet apex to the 86 GHz intensity peak is $0.028 - 0.11$ pc, or $400 - 1500 R_s$ (assuming a black hole mass of $9 \times 10^8 M_\odot$ [26]).

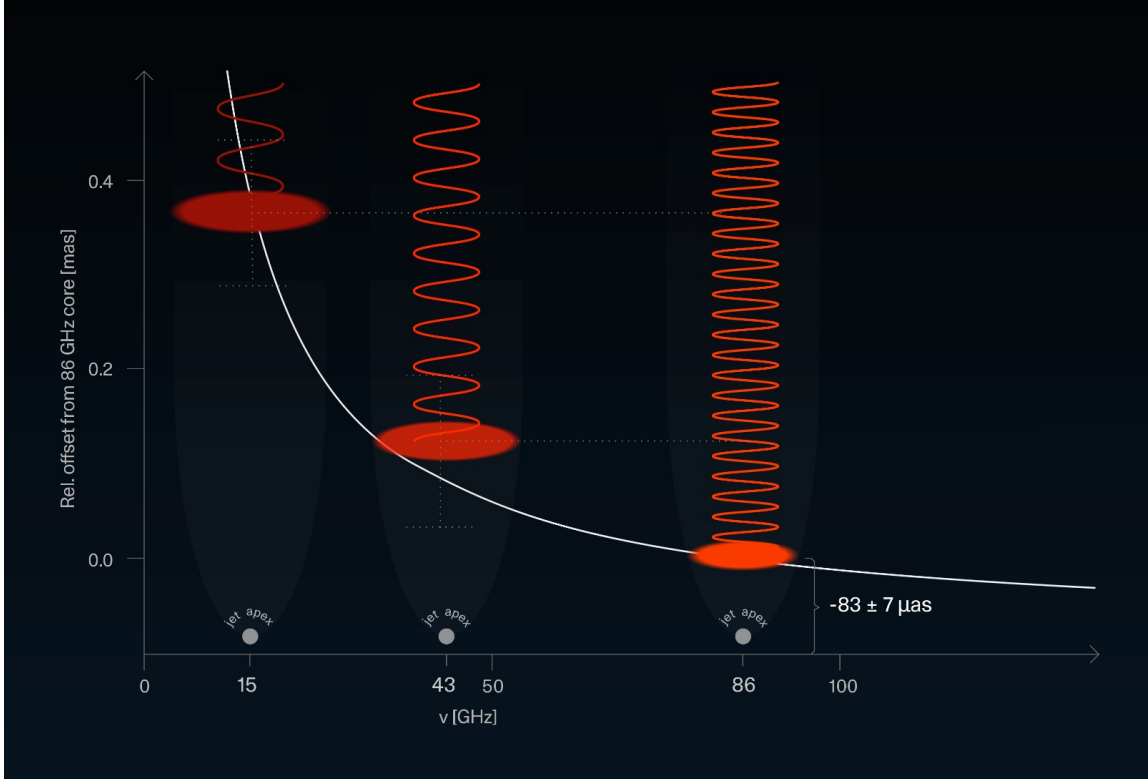


Figure 2: Position offset of the 15 and 43 GHz intensity peaks in the core region relative to the 86 GHz intensity peak, as a function of frequency. The grey continuous line displays the fit of Eq. 1 to the data points. The distance of the jet apex (denoted with grey disks) to the 86 GHz intensity peak is found to be $83 \pm 7 \mu\text{as}$. The red/orange ellipses showcase the observed core at different wavelengths/frequencies, illustrating the concept of the core shift.

3. Spectral index

A byproduct of the cross-correlation analysis are spectral index maps. Here we define the spectral index as $S \propto \nu^{+\alpha}$. For the analysis we focus on the two adjacent frequency pairs, because the large difference in beam size between 15 and 86 GHz causes beam blending effects.

Figure 4 illustrates different scenarios for the appearance of spectral index maps of the nuclear region, depending on the underlying physical model. Starting from the top and in clockwise direction: (i) for a black hole at the center surrounded by a uniform disk one may expect a relatively uniform, flattish spectral index distribution. (ii) A Blandford & Payne powered jet [27] would lead to an edge brightened jet, manifesting in a steep spectral index east and west of the black hole, and flat at the center. (iii) An upstream located black hole would produce a smooth gradient in the north-south direction. (iv) An identification of the VLBI core as a recollimation shock (at some arbitrary distance from the BH) would lead to a flat to moderately steep spectral index. (v) Finally, if the black hole is located at the western edge of the jet (c.f. [28]) and if the inner (sub-mas) jet is strongly misaligned with the mas-scale jet, we would expect a spectral index gradient in the east-west direction.

In Fig. 5 we present our spectral index analysis. The presence of a north-south oriented spectral

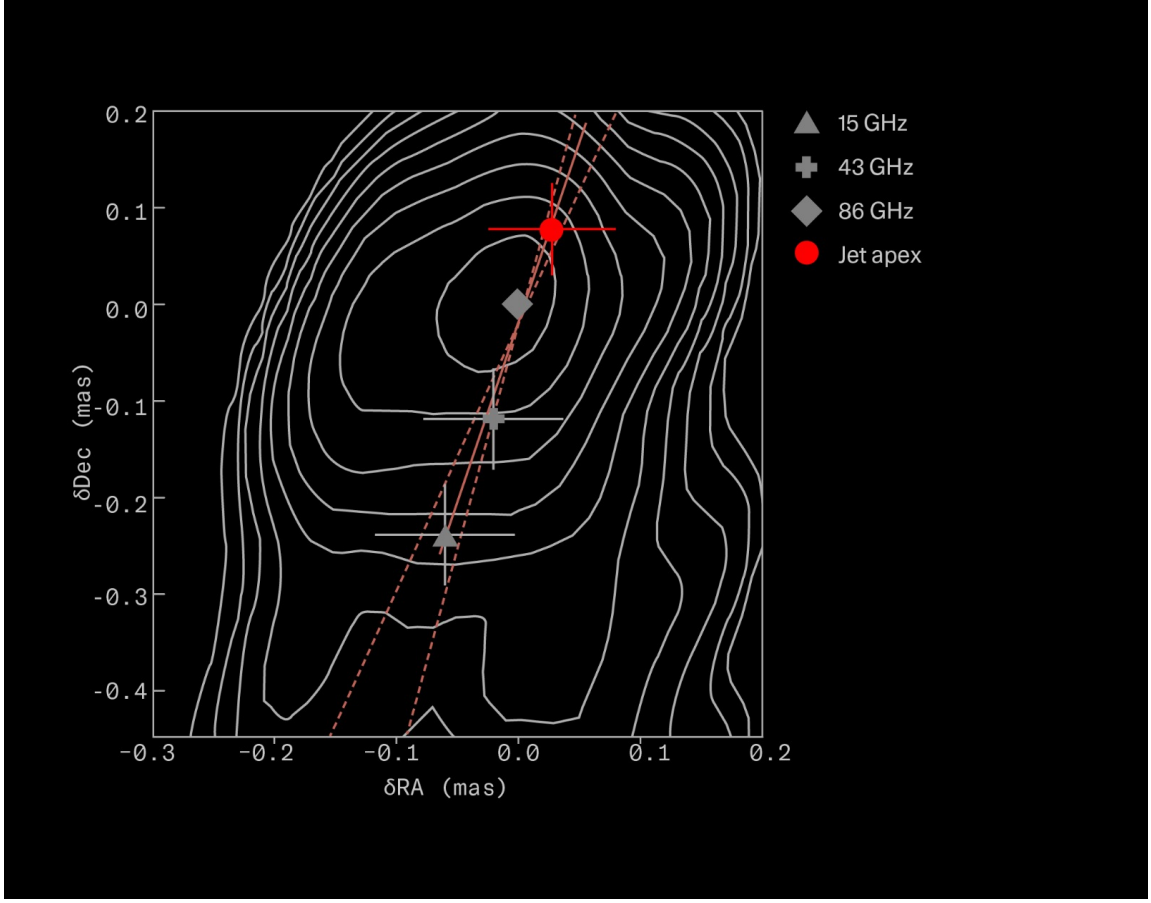


Figure 3: Intensity peaks at 15, 43, 86 GHz and extrapolated jet apex. The intensity peaks are denoted with the grey symbols, the jet apex with the red dot. They are super-imposed on 86 GHz image contours, which start at 0.1% of the image peak (1.82 Jy/beam) and then increase in steps of two. The solid red line marks the extrapolated jet flow direction and the dashed red lines outline the 99% confidence interval of the fit.

index gradient is obvious from both frequency pairs. We note the measurement of the spectral index gradient at 43-86 GHz for the first time and at such high angular resolution. Comparing our results to the illustrations of Fig. 4, they appear consistent with a jet apex location north of the 86 GHz VLBI core and consequently a black hole location upstream of the visible portion of the jet.

4. Magnetic field

Utilising a number of assumptions, namely that the jet is described by the Blandford & Königl model [29], and is synchrotron self-absorbed, we can compute the magnetic field, as described in [19, 22]. At the extrapolated jet apex location, we estimate the magnetic field to be $\sim 2 - 4$ G (see [30] for more details). We can also compare our result to other prominent AGN, if we extrapolate the magnetic field strength closer to the BH location (cf. [30]), for example to $\approx 10 R_s$. At this distance the magnetic field $B_{10 R_s}$ is 70 – 600 G, which compares well to M87 and NGC 1052 [31, 32]. We note that a lower frequencies (15 GHz), a total of ~ 100 quasar and BL Lac jets were analysed by [21]. Based on their core shifts, an average magnetic field strength of $\sim 400 - 900$ mG was obtained,

THE JET BASE OF 3C 84

Model discrimination via Spectral Index Mapping

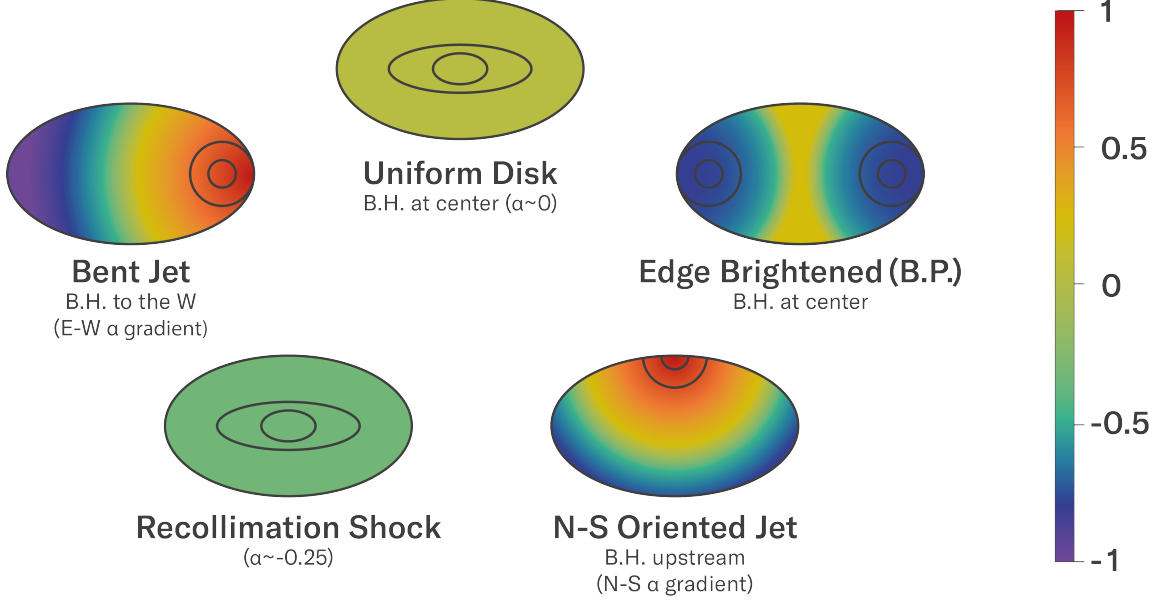


Figure 4: Illustration of the expected spectral index, depending on the location and true nature of the VLBI core of 3C 84.

at a distance of 1 pc from the jet apex. In 3C 84, the magnetic field at the same distance from the core amounts to 60 – 180 mG, which is 4 – 6 times lower than the typical magnetic fields of the AGN studied by [21].

Besides the magnetic field strength, we also may set some constraints on its configuration. Our analysis points to a mixed toroidal/poloidal configuration ($b \approx 1.7$), with the assumption that the total number of particles passing through each cross-section is conserved, and using the result by [24] that the jet radius R and the distance to the core z are connected by a power-law of the form $z \propto R^{0.21}$.

The visual appearance of an edge-brightened inner jet suggests transverse jet stratification, which is a natural consequence, for example from a combination of the Blandford & Payne and a Blandford & Znajek [33] jet launching scenarios. Overall, the magnetic field appears strong near the BH, compared to the upper limit estimation (see Eq. 8.35 in [34]) from the total jet power [25, 35], in support of magnetic jet launching [36, 37].

5. Conclusions

1. The black hole in 3C 84 is located $\geq 400\text{-}1500 R_s$ upstream of the 86 GHz VLBI core.
2. A strong spectral index gradient in north-south direction is discovered, rendering 3C 84 a suitable target for core-shift analysis including the highest VLBI frequencies.

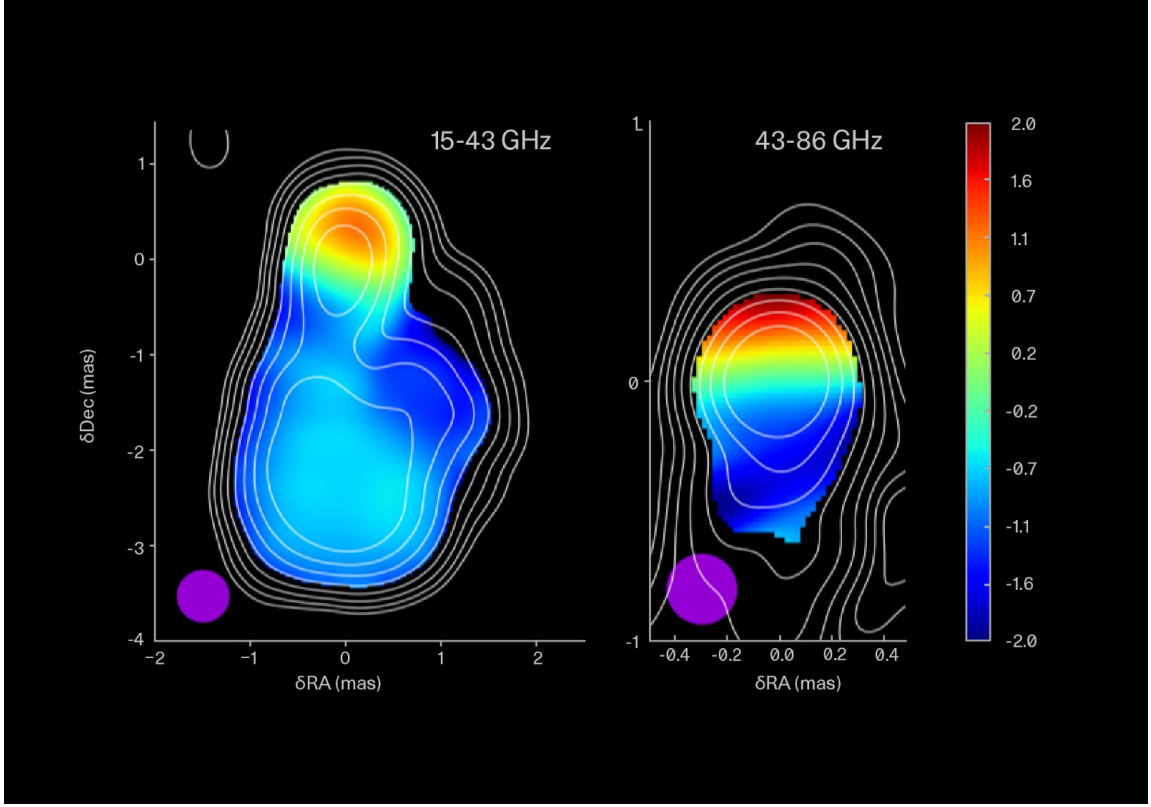


Figure 5: Spectral index maps of 3C 84 at 15-43 GHz and 43-86 GHz. A prominent spectral index in the north-south direction is revealed. Left: 15-43 GHz spectral index map, super-imposed on the 15 GHz total intensity contours. Right: 43-86 GHz spectral index map, super-imposed on the 43 GHz total intensity contours.

3. The magnetic field at $10 R_s$ is computed to be 70-600 G, which compares well with other nearby radio galaxies, such as M 87 or NGC 1052.
4. At distances comparable to the jet apex, we found a mixed poloidal-toroidal magnetic field configuration, pointing perhaps to a stratified combination of Blandford & Payne and Blandford & Znajek jet launching mechanism.

The above analysis and results are described in more detail in [30].

6. Outlook

Although our results put new limits on the location of the jet apex and the BH in 3C 84, the opening angle of the inner jet and the polarisation at the jet base are not yet unambiguously determined. The accurate determination of the inner jet velocity and the direction of the component motion is yet another important topic. Further VLBI imaging observations with sufficient high angular resolution (GMVA at 43/86 GHz, EHT at 230/345 GHz) will address these topics. Specifically, already planned quasi-simultaneous observations at 22 and 43 GHz with the Global-EVN and 86

and 230 GHz observations with the GMVA and EHT should yield better polarimetric data, providing a more detailed insight into the magnetic field properties for the inner jet region in 3C 84.

Acknowledgments

We thank T. Savolainen for providing software to calculate two dimensional cross-correlations. This work makes use of 15, 37 GHz and 230 GHz light curves kindly provided by the Owen’s Valley Radio Observatory, Metsähovi Radio Observatory and the Submillimeter Array, respectively. G. F. Paraschos is supported for this research by the International Max-Planck Research School (IMPRS) for Astronomy and Astrophysics at the University of Bonn and Cologne. This research has made use of data obtained with the Global Millimeter VLBI Array (GMVA), which consists of telescopes operated by the MPIfR, IRAM, Onsala, Metsähovi, Yebes, the Korean VLBI Network, the Green Bank Observatory and the VLBA (NRAO). The Submillimeter Array (SMA) is a joint project between the Smithsonian Astrophysical Observatory and the Academia Sinica Institute of Astronomy and Astrophysics and is funded by the Smithsonian Institution and the Academia Sinica. This research has also made use of data from the Owen’s Valley Radio Observatory 40-m monitoring program [16], supported by private funding from the California Institute of Technology and the Max Planck Institute for Radio Astronomy, and by NASA grants NNX08AW31G, NNX11A043G, and NNX14AQ89G and NSF grants AST-0808050 and AST-1109911. Finally, this research makes use the publicly available γ -ray light curve of NGC 1275 (https://fermi.gsfc.nasa.gov/ssc/data/access/lat/msl_lc/source/NGC_1275).

References

- [1] W. Baade and R. Minkowski, *On the Identification of Radio Sources.*, **ApJ** **119** (1954) 215.
- [2] R. C. Walker, V. Dhawan, J. D. Romney, K. I. Kellermann and R. C. Vermeulen, *VLBA Absorption Imaging of Ionized Gas Associated with the Accretion Disk in NGC 1275*, **ApJ** **530** (2000) 233 [[astro-ph/9909365](#)].
- [3] V. Dhawan, N. Bartel, A. E. E. Rogers, T. P. Krichbaum, A. Witzel, D. A. Graham et al., *Further 7 Millimeter VLBI Observations of 3C 84 and Other Sources with 100 Microarcsecond Angular Resolution*, **ApJ** **360** (1990) L43.
- [4] T. P. Krichbaum, A. Witzel, D. A. Graham, W. Alef, I. I. K. Pauliny-Toth, C. A. Hummel et al., *The evolution of the sub-parsec structure of 3C 84 at 43 GHz.*, **A&A** **260** (1992) 33.
- [5] H. Nagai, T. Haga, G. Giovannini, A. Doi, M. Orienti, F. D’Ammando et al., *Limb-brightened Jet of 3C 84 Revealed by the 43 GHz Very-Long-Baseline-Array Observation*, **ApJ** **785** (2014) 53 [[1402.5930](#)].
- [6] J. A. Hodgson, B. Rani, J. Oh, A. Marscher, S. Jorstad, Y. Mizuno et al., *A Detailed Kinematic Study of 3C 84 and Its Connection to γ -Rays*, **ApJ** **914** (2021) 43 [[2104.03081](#)].
- [7] W. A. Dent, *Variation in the Radio Emission from the Seyfert Galaxy NGC 1275*, **ApJ** **144** (1966) 843.

- [8] R. C. Vermeulen, A. C. S. Readhead and D. C. Backer, *Discovery of a Nuclear Counterjet in NGC 1275: A New Way to Probe the Parsec-Scale Environment*, [ApJ **430** \(1994\) L41](#).
- [9] R. C. Walker, J. D. Romney and J. M. Benson, *Detection of a VLBI Counterjet in NGC 1275: A Possible Probe of the Parsec-Scale Accretion Region*, [ApJ **430** \(1994\) L45](#).
- [10] Y. Fujita and H. Nagai, *Discovery of a new subparsec counterjet in NGC 1275: the inclination angle and the environment*, [MNRAS **465** \(2017\) L94 \[1609.04017\]](#).
- [11] K. Wajima, M. Kino and N. Kawakatu, *Constraints on the Circumnuclear Disk through Free-Free Absorption in the Nucleus of 3C 84 with KaVA and KVN at 43 and 86 GHz*, [ApJ **895** \(2020\) 35 \[2004.06589\]](#).
- [12] J. Y. Kim, T. P. Krichbaum, A. P. Marscher, S. G. Jorstad, I. Agudo, C. Thum et al., *Spatially resolved origin of millimeter-wave linear polarization in the nuclear region of 3C 84*, [A&A **622** \(2019\) A196 \[1811.07815\]](#).
- [13] V. Dhawan, K. I. Kellermann and J. D. Romney, *Kinematics of the Nucleus of NGC 1275 (3C 84)*, [ApJ **498** \(1998\) L111](#).
- [14] S. Britzen, C. Fendt, M. Zajaček, F. Jaron, I. Pashchenko, M. F. Aller et al., *3C 84: Observational Evidence for Precession and a Possible Relation to TeV Emission*, [Galaxies **7** \(2019\) 72](#).
- [15] L. Linhoff, A. Sandrock, M. Kadler, D. Elsässer and W. Rhode, *Excluding possible sites of high-energy emission in 3C 84*, [MNRAS **500** \(2021\) 4671](#).
- [16] J. L. Richards, W. Max-Moerbeck, V. Pavlidou, O. G. King, T. J. Pearson, A. C. S. Readhead et al., *Blazars in the Fermi Era: The OVRO 40 m Telescope Monitoring Program*, [ApJS **194** \(2011\) 29 \[1011.3111\]](#).
- [17] Fermi Large Area Telescope Collaboration, *10-year Fermi LAT point source catalog*, *The Astronomer's Telegram* **15110** (2021) 1.
- [18] G. B. Rybicki and A. P. Lightman, *Radiative processes in astrophysics*. 1979.
- [19] A. P. Lobanov, *Spectral distributions in compact radio sources. I. Imaging with VLBI data*, [A&AS **132** \(1998\) 261 \[astro-ph/9804112\]](#).
- [20] K. Hada, A. Doi, M. Kino, H. Nagai, Y. Hagiwara and N. Kawaguchi, *An origin of the radio jet in M87 at the location of the central black hole*, [Nature **477** \(2011\) 185](#).
- [21] A. B. Pushkarev, T. Hovatta, Y. Y. Kovalev, M. L. Lister, A. P. Lobanov, T. Savolainen et al., *MOJAVE: Monitoring of Jets in Active galactic nuclei with VLBA Experiments. IX. Nuclear opacity*, [A&A **545** \(2012\) A113 \[1207.5457\]](#).
- [22] C. M. Fromm, E. Ros, M. Perucho, T. Savolainen, P. Mimica, M. Kadler et al., *Catching the radio flare in CTA 102. III. Core-shift and spectral analysis*, [A&A **557** \(2013\) A105 \[1306.6208\]](#).

- [23] J. Oh, J. A. Hodgson, S. Trippe, T. P. Krichbaum, M. Kam, G. F. Paraschos et al., *A persistent double nuclear structure in 3C 84*, [*MNRAS* **509** \(2022\) 1024 \[2110.09811\]](#).
- [24] G. Giovannini, T. Savolainen, M. Orienti, M. Nakamura, H. Nagai, M. Kino et al., *A wide and collimated radio jet in 3C84 on the scale of a few hundred gravitational radii*, [*Nature Astronomy* **2** \(2018\) 472 \[1804.02198\]](#).
- [25] A. A. Abdo, M. Ackermann, M. Ajello, K. Asano, L. Baldini, J. Ballet et al., *Fermi Discovery of Gamma-ray Emission from NGC 1275*, [*ApJ* **699** \(2009\) 31 \[0904.1904\]](#).
- [26] J. Scharwächter, P. J. McGregor, M. A. Dopita and T. L. Beck, *Kinematics and excitation of the molecular hydrogen accretion disc in NGC 1275*, [*MNRAS* **429** \(2013\) 2315 \[1211.6750\]](#).
- [27] R. D. Blandford and D. G. Payne, *Hydromagnetic flows from accretion disks and the production of radio jets.*, [*MNRAS* **199** \(1982\) 883](#).
- [28] B. Punsly, H. Nagai, T. Savolainen and M. Orienti, *Observing the Time Evolution of the Multicomponent Nucleus of 3C 84*, [*ApJ* **911** \(2021\) 19 \[2102.07272\]](#).
- [29] R. D. Blandford and A. Königl, *Relativistic jets as compact radio sources.*, [*ApJ* **232** \(1979\) 34](#).
- [30] G. F. Paraschos, J. Y. Kim, T. P. Krichbaum and J. A. Zensus, *Pinpointing the jet apex of 3C 84*, [*A&A* **650** \(2021\) L18 \[2106.04918\]](#).
- [31] J. Y. Kim, T. P. Krichbaum, R. S. Lu, E. Ros, U. Bach, M. Bremer et al., *The limb-brightened jet of M87 down to the 7 Schwarzschild radii scale*, [*A&A* **616** \(2018\) A188 \[1805.02478\]](#).
- [32] A. K. Baczko, R. Schulz, M. Kadler, E. Ros, M. Perucho, T. P. Krichbaum et al., *A highly magnetized twin-jet base pinpoints a supermassive black hole*, [*A&A* **593** \(2016\) A47 \[1605.07100\]](#).
- [33] R. D. Blandford and R. L. Znajek, *Electromagnetic extraction of energy from Kerr black holes.*, [*MNRAS* **179** \(1977\) 433](#).
- [34] G. Ghisellini, *Radiative Processes in High Energy Astrophysics*, vol. 873. 2013, [10.1007/978-3-319-00612-3](#).
- [35] MAGIC Collaboration, S. Ansoldi, L. A. Antonelli, C. Arcaro, D. Baack, A. Babić et al., *Gamma-ray flaring activity of NGC1275 in 2016-2017 measured by MAGIC*, [*A&A* **617** \(2018\) A91 \[1806.01559\]](#).
- [36] R. Narayan, I. V. Igumenshchev and M. A. Abramowicz, *Magnetically Arrested Disk: an Energetically Efficient Accretion Flow*, [*PASJ* **55** \(2003\) L69 \[astro-ph/0305029\]](#).
- [37] A. Tchekhovskoy, R. Narayan and J. C. McKinney, *Efficient generation of jets from magnetically arrested accretion on a rapidly spinning black hole*, [*MNRAS* **418** \(2011\) L79 \[1108.0412\]](#).